[c5]Electron curtain precipitation is observed in low Earth orbit (LEO) and appears stationary in latitude. Curtains were recently discovered by Blake and O'Brien (2016) using the > 35 keV electron dosimeters onboard the dual AeroCube-6 (AC6) CubeSats that operated together between 2014 and 2017. Curtains are narrow in latitude and persist for up to a minute between subsequent satellite passes [c6](our estimate of the curtain lifetime is ultimately limited by the AC6 separation). This discovery was made possible by AC6's actively maintained in-track separation that varied between a few hundred meters and a few hundred kilometers. Besides the Blake and O'Brien (2016) study, not much is known about curtains including what they are, how are they generated, and their impact on the atmosphere. Answering these questions is an essential next step towards a more complete understanding of how curtains, and particle precipitation in general, affect the magnetosphere and Earth's atmosphere.

In low Earth orbit, curtains are narrower than a few tens of kilometers in the latitudinal direction. A polar-orbiting LEO satellite, such as AC6, will pass through the curtain cross-section in a few seconds, which appears in the electron count time series as short enhancements in flux. AC6 also observes similar-looking transient precipitation called electron microbursts. Curtains and microbursts are observed in the AC6 data but appear short-lived for different reasons: microbursts are temporal, while curtains are spatial. Hence AC6, and other recently developed multi-spacecraft missions, are necessary to identify and distinguish between transient microbursts and the persistent curtains.

Since the mid-1960s, microbursts have been observed by high altitude balloons where they appear as sharp peaks in flux with a sub-second duration (e.g. K. A. Anderson & Milton, 1964; R. Brown et al., 1965; Parks, 1967). Because balloons are relatively stationary, a microburst is easily classified as a transient phenomenon. Microburst electrons have also been directly observed by LEO satellites such as The Solar Anomalous and Magnetospheric Particle Explorer (e.g. Blake et al., 1996; Lorentzen, Blake, et al., 2001; O'Brien et al., 2003; Douma et al., 2017). But a flux enhancement that looks like a microburst from a single LEO satellite is ambiguous—it can be transient or it can be persistant, stationary, and narrow in latitude. Thus, multi-spacecraft missions such as the Focused Investigations of Relativistic Electron Burst Intensity, Range, and Dynamics (FIREBIRD-II) (Crew et al., 2016; Johnson et al., 2020) and AC6 (Blake & O'Brien, 2016; O'Brien et al., 2016) are necessary to resolve the temporal vs. spatial ambiguity. [c1]In a case study, B. Anderson et al. (2017) [c2]used the Balloon Array for Radiation-belt Relativistic Electron Losses (BARREL), together with AC6 and FIREBIRD-II CubeSats to resolve the spatial and temporal ambiguity of the macroscopic microburst and curtain precipitation region. B. Anderson et al. (2017) [c3]found that microbursts occur over an L shell range between 5 and 10 and between 9 and 13 hours magnetic local time (MLT). In addition, the authors found that curtains and microbursts were observed together during the same radiation belt pass. While this study focuses on curtain precipitation, microburst precipitation observed across the dawn sector by AC6 was studied in Shumko et al. (2020).

While the impact of curtains on the magnetosphere and Earth's atmosphere is unknown, the impact of microbursts has been estimated to be substantial. Lorentzen, Looper, and Blake (2001), Thorne et al. (2005), Breneman et al. (2017), and Douma et al. (2019), among others, estimated that microbursts could deplete the outer radiation belt electrons in about a day. Furthermore, Seppälä et al. (2018) modeled a 6-hour microburst storm and concluded that microbursts depleted mesospheric ozone by roughly 10%. Mi-

[c5] ~~Electron curtain precipitation is a stationary phenomenon observed in low Earth orbit (LEO).~~
[c6] *Text added.*
[c1] *Text added.*
[c2] *Text added.*
[c3] *Text added.*

107 crobursts and curtains can be easily misidentified from a single satellite; if curtains are
108 numerous, then the atmospheric and magnetospheric impact associated with microburst
109 observations from single satellites may be overestimated.

110 Precipitation bands, sometimes also referred to as spikes (e.g. Imhof et al., 1991),
111 are [c1] a similar form of precipitation. [c2] Precipitation bands also appear as stationary
112 and narrow flux enhancements with a > 1 second duration, and can persist from an hour
113 to as much as half a day (e.g. J. Brown & Stone, 1972; Blake et al., 1996). Blum et al.
114 (2013) identified two precipitation bands and estimated that only 20 precipitation bands
115 can deplete all of the outer radiation belt electrons. The mechanism responsible for scat-
116 tering precipitation band electrons at high L is believed to be field line curvature scat-
117 tering, but the scattering mechanism for band electrons at lower L shells is unknown.
118 A few proposed scattering mechanisms include wave-particle interactions and acceler-
119 ation due to parallel direct current potentials (Hoffman & Evans, 1968). [c3] Precipitation
120 bands and curtains could be related. However, a comparison with existing observations
121 is difficult because the most recent, and the most comparable, precipitation band stud-
122 ies looked at relativistic precipitation bands—a very different energy regime from AC6.

123 [c4] The apparent curtain fine structure that persist for multiple seconds can be
124 be explained by at least two mechanisms. In the first mechanism, curtain electrons
125 are scattered via gyroresonant interactions with chorus waves and initially produce a
126 bounce phase structure—a bouncing packet. During subsequent bounces, the bouncing
127 packet structure is dispersed along the bounce path, and is then observed by AC6's
128 integral channel downstream as a stable structure. Alternately, on the local field line,
129 pitch angle transport occurs independent of bounce phase so these particles do not
130 necessarily have to be drifting. The two AC6 spacecraft then pass through the same
131 field line while the source is active. We will return to the second hypothesized mecha-
132 nism later, and for now focus on the first mechanism that was proposed by Blake and
133 O'Brien (2016).

134 Blake and O'Brien (2016) proposed a hypothesis that curtains are drifting remnants
135 of microbursts. If a microburst is not completely lost in the atmosphere after the ini-
136 tial scatter, the remaining microburst electrons will spread out (bounce phase disperse)
137 along the entire magnetic field line over a few bounce periods. Concurrently these elec-
138 trons drift to the east, with higher energy electrons drifting at a faster rate. Assuming
139 this hypothesis, the initially localized microburst is spread out in longitude into the shape
140 of a curtain. A similar phenomena was hypothesized by Lehtinen et al. (2000) who pre-
141 dicted that drifting curtains can be created by energetic runaway beams driven by light-
142 ning, but these curtains would be observed at relatively low L shells. [c5] The curtain shape
143 and nomenclature are a direct consequence of the above untested hypotheses; however,
144 the true shape of the precipitation studied here is unknown. To be consistent with
145 Blake and O'Brien (2016), [c6] we also adopt the curtain nomenclature, but we stress
146 the need to be cognizant of other possible realities and not let the curtain concept bias
147 our interpretations.

148 This study expands on Blake and O'Brien (2016) by examining the statistical prop-
149 erties of curtains. We use 1,634 confirmed curtain observations to study the distributions
150 of the curtain: width in latitude, the geomagnetic conditions favorable to curtains, [c7] the
151 occurrence frequencies in latitude-longitude, and the occurrence frequencies in L and

[c1] ~~another~~
[c2] ~~that could be related to curtains~~
[c3] *Text added.*
[c4] *Text added.*
[c5] *Text added.*
[c6] *Text added.*
[c7] *Text added.*

MLT. Lastly we will show examples of curtains that continuously precipitated in the bounce loss cone (BLC) region.

2 Instrumentation

The AC6 mission was a pair of 0.5U (10x10x5 cm) CubeSats built by The Aerospace Corporation and designed to measure the electron and proton environment in low Earth orbit (O'Brien et al., 2016). AC6 was launched on 19 June 2014 into a 620x700 km, 98° inclination orbit. The AC6 orbit over the three year mission lifetime was roughly dawn-dusk, and precessed only a few hours in MLT: 8-12 MLT in the dawn and 20-24 MLT in the dusk sectors. The two AC6 spacecraft, designated as AC6-A and AC6-B, separated after launch and were in proximity for the duration of the three-year mission—maintained by an active attitude control system. The attitude control system allowed them to actively control the amount of atmospheric drag experienced by each AC6 unit using the surface area of their solar panel "wings." By changing their orientation, AC6 was able to maintain a separation between 2-800 km, confirmed by the Global Positioning System. The two AC6 units were in a string of pearls configuration, so one unit, typically unit A, was leading the other by an in-track lag: the time it would take the following spacecraft to catch up to the position of the leading spacecraft. To convert between the AC6 in-track separation and in-track lag, the AC6 orbital velocity was used. AC6's orbital velocity was 7.6 km/s and varied by as much as 0.1 km/s. The in-track lag is readily available in the data files with the Global Positioning System, which makes it possible to remove the spatiotemporal ambiguity that affects single-spacecraft measurements.

Each AC6 unit contains three Aerospace microdosimeters (licensed to Teledyne Microelectronics, Inc) that measure the electron and proton dose in orbit (O'Brien et al., 2016). The dosimeter used for this study is dos1 with a > 35 keV integral electron response, as the other dosimeters either responded primarily to protons or were not identical between unit A and B. All dosimeters sample at 1 Hz in survey mode, and 10 Hz in burst mode. 10 Hz data is available from both AC6 units from June 2014 to May 2017 while their in-track lag was less than 65 seconds. Figure A1 in the appendix shows the distribution of 10 Hz data as a function of AC6 in-track lag.

3 Methodology

3.1 Curtain Identification

The 10 Hz data were used to identify curtains using the following two criteria: a high spatial correlation, and a prominent peak. Before we applied the identification criteria, the AC6-B time series was shifted by the in-track lag to spatially align it with the AC6-A time series.

The first identification criterion is a 1-second rolling Pearson correlation applied to both time series. Spatial features with a correlation greater than 0.8 are considered highly correlated. The second criterion is applied to the highly correlated features to check if they are also prominently peaked. To find peaked precipitation, we used a technique similar to the technique used by Blum et al. (2015) to identify precipitation bands, and by Greeley et al. (2019) to identify microbursts. Our technique quantified the number of Poisson standard deviations, σ, that dos1 counts in each 100 ms bin are above a 10-second centered running average, b_{10}. Locations where dos1 counts are at least two σ above b_{10}, in other words $dos1 > 2\sqrt{b_{10}}+b_{10}$, are considered prominently peaked. One bias inherent to this detection algorithm, and similar algorithms such as the burst parameter (O'Brien et al., 2003), is a reduced sensitivity for wider peaks. For curtains with a width similar to b_{10}, the baseline will be significantly elevated making the curtain peak

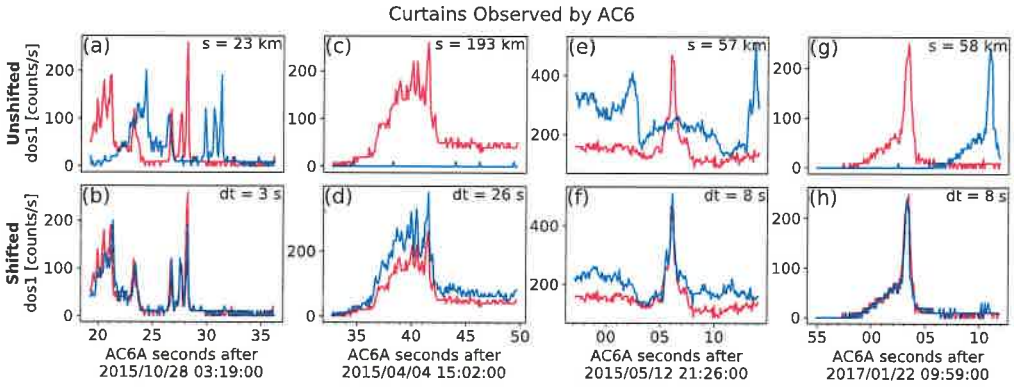

Figure 1. Four examples showing the > 35 keV electron time series data taken by AC6 at the same time (unshifted) in the top row and at the same position (shifted) in the bottom row, with curtains clearly visible in the bottom row. AC6-A, whose data is shown with the red curves, was s kilometers ahead of AC6-B. To show the data at the same position the AC6-B time series was shifted by the in-track lag annotated by dt. These examples show that curtain precipitation was highly correlated for up to 26 seconds.

less pronounced. [c1] This bias will be revisited later, but one generalization of this method is to use a set different baseline widths and aggregate the resulting detections.

We tuned the automated detection parameters to identify a large number of curtains. Once curtains were automatically identified, one author visually inspected 6,149 candidate curtains and verified 1,634 curtains, [c1] prior to generating the analysis. The visual inspection was performed to remove ambiguous detections where the peaks lined up in [c2] both space and time, and false positive detections that were triggered by three conditions: sharp count rate shoulders, low baseline (b_{10}), and high correlations resulting from Poisson noise. Four curtain examples are shown in Fig. 1. In each instance, the unmodified time series is shown in the top row and the spatially-aligned time series in the bottom row. The in-track lag used to shift the bottom row is annotated by dt, corresponding to an AC6 in-track separation annotated by s. The bottom row shows highly correlated curtains observed at the same location for at least 3 to 26 seconds.

3.2 Differentiating Between Drifting and Precipitating Curtains

The AC6 dosimeters lack the necessary pitch angle resolution to differentiate between locally drifting and precipitating electrons to test the Blake and O'Brien (2016) hypothesis that curtains are the drifting remnants of microbursts. Fortunately, one standard method of distinguishing between locally precipitating, drifting, and trapped particles is by using the geographic location of observations with respect to the location of the South Atlantic Anomaly (SAA).

Earth's magnetic field is asymmetric and has a region of weaker magnetic field in the South Atlantic Ocean called the South Atlantic Anomaly. The weaker magnetic field in the SAA naturally differentiates particles by pitch angle into trapped and quasi-trapped

[c1] *Text added.*
[c1] *Text added.*
[c2] *Text added.*

populations. While some particles observed in LEO are trapped and will execute closed drift paths, most particles observed in LEO are quasi-trapped: they drift around the Earth until they reach the SAA. Within the SAA, the weaker magnetic field strength can lower the particle's mirror point altitude into the atmosphere, where collisions with the atmospheric neutrals and ions are more numerous and the particle is lost.

Particles that are quasi-trapped have pitch angles in the drift loss cone and will precipitate within one drift period (often within the SAA). Particles with smaller equatorial pitch angles that are lost in the atmosphere within one bounce are in the bounce loss cone (BLC). Traditionally, a particle is in the BLC if its mirror point altitude is at or below 100 km in either hemisphere (e.g. Selesnick et al., 2003).

In most regions outside of the SAA and its conjugate point in the North Atlantic, AC6 will observe a combination of drift and bounce loss cone electrons. In the SAA, AC6 does not only observe electrons that are immediately lost, but a combination of electrons that are in the drift loss cone, bounce loss cone, and trapped (a trapped electron that locally mirrors at AC6's altitude in the SAA will mirror at higher altitudes everywhere else). In the region magnetically conjugate to the SAA in the North Atlantic, AC6 only observes electrons in the BLC. Here, if an electron makes it to AC6's altitude, it might be in the local loss cone and precipitate in the local hemisphere. Alternatively, the electron may mirror at or below AC6 and bounce to its conjugate mirror point deep in the atmosphere or below sea level in the SAA. Therefore, any electrons observed in the BLC region will likely precipitate within one bounce ($\approx$ 1.5 seconds for 35 keV electrons).

We estimated the BLC region for locally-mirroring electrons in the North Atlantic Ocean using the IRBEM-Lib magnetic field library and the Olson-Pfitzer magnetic field model (Boscher et al., 2012; Olson & Pfitzer, 1982). We defined a latitude-longitude grid, with a $\approx 0.5° \times 0.5°$ grid size, spanning the North Atlantic at 700-kilometers altitude, and estimated the local magnetic field strength. The 700-kilometers altitude was chosen because it is the upper bound altitude for AC6's orbit and it is the conservative limit because at lower altitudes the BLC region is larger. For each latitude-longitude point we traced the magnetic field line to the southern hemisphere and found the conjugate mirror point altitude. If the conjugate mirror point is $\leq$ 100 kilometers, the electron is likely lost and the associated grid point is in the BLC. Furthermore, a more rigorous bounce loss cone criterion is the conjugate mirror point altitude below sea level. In this case, the electron is very likely lost. The BLC region estimated by this method closely matches the BLC region shown in Comess et al. (2013, Figure 1) and Dietrich et al. (2010, Figure 3) for other LEO satellites. Lastly, we repeated the same analysis using the Tsyganenko 1989 model (Tsyganenko, 1989), which yielded similar BLC boundaries.

4 Results

In this study we addressed three questions: what is the distribution of curtain widths along the AC6 orbit (mostly in geographic latitude), when and where are curtains observed, and are curtains composed of drifting or locally precipitating electrons?

4.1 Curtain Width

The curtain width is quantified as the width at half of the curtain's topographic prominence, as described in Appendix B. The spatial width of a curtain is then the product of the observed width in time and AC6's orbital velocity. The curtain width is measured along AC6's orbit track which is mostly in the latitudinal direction, therefore the estimated curtain widths are also mostly in the latitudinal direction. The distribution of curtain widths is shown in Fig. 2. Curtains are very narrow. Many curtains are narrower than 10 km in the latitudinal direction, and 90% are narrower than 20 km.

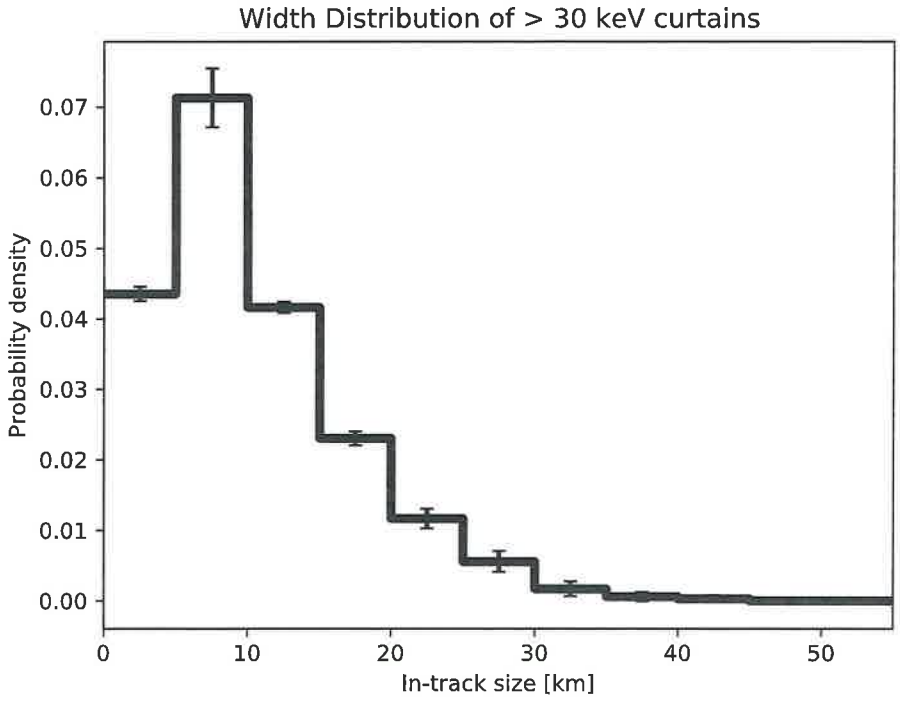

Figure 2. The distribution of curtain widths along the AC6 orbit. The error bars are derived assuming the Poisson standard error.

?

In this and other PDF often more useful to not divide by b.w width. I.e. most prominent b.w is 35% of widths

poisson error on dose?

or on number of events in each b.w? If the latter it seems strange that largest relative error is in most prominent b.w.

Also, weird normalization? Integration to much less than 1?

4.2 When and Where Are Curtains Observed

The distribution of curtains in L and MLT is shown in Fig. 3. Figure 3a shows the distribution of the observed curtains, while Fig. 3b shows the same distribution normalized by the number of quality 10 Hz samples (flag = 0 in the data files) that both AC6 spacecraft took at the same location in each L-MLT bin. In Fig. 3a and 3b, the bins where no curtains were observed are white. The AC6 sampling distribution is shown in Fig. 3c, whose white bins show where AC6 did not take any 10 Hz data at the same location. The normalized curtain distribution in Fig. 3b shows an enhanced curtain occurrence in the radiation belts [c1] and the plasma sheet ($L \approx 5 - 10$) with the largest peak in the pre-midnight MLT sector. [c2] Since the AC6 dosimeters are sensitive to > 35 keV electrons, these curtains can have electron energies as low as ≈ 35 keV and can also be associated with the upper energy end of the ring current or auroral precipitation.

[c3] The normalized geographic distribution of curtains is shown in Fig. 4a [c4] and the marginalized distributions are shown in Fig. 4b,c. [c5] Fig. 4a [c6] shows that curtains are distributed roughly uniformly around the Earth. Furthermore, this distribution leads to the following three insights. First, the North-South asymmetry seen in Fig. 4b [c7] is due to the higher occurrence rate of curtains in the North Atlantic region (the bounce loss cone region). Second, Fig. 4c [c8] shows that curtains are distributed roughly uniformly in longitude. Third, the number of curtains observed in the outer belt SAA in Fig. 4a [c9] is low. This is a consequence of the higher background in the SAA due to the trapped population—a curtain is less pronounced when the background is high.

We also examine the geomagnetic conditions favorable for curtains. [c10] Many prior wave and precipitation studies such as Douma et al. (2019) and Meredith et al. (2020) [c11] quantified the geomagnetic conditions with the Auroral Electrojet (AE) index. Therefore, we also use the AE index. Figure 5a shows the distribution of the minute cadence AE index between 2014 and 2017 in solid black, for times when quality 10 Hz data were available from both AC6 units. Furthermore, the distribution of the AE index when curtains were observed is shown by the solid blue lines. Curtains are observed during both low and high geomagnetic activity, slightly more often at higher AE than the index itself (curtain distribution trends above the AE index when $AE > 200$). Lastly, we normalized the curtain distribution in Fig. 5a assuming any AE index is equally probable. The normalized curtain distribution is shown in Fig. 5b, which emphasizes that the curtain occurrence frequency increases with increasing AE index up to ≈ 600 nT.

4.3 Local Atmospheric Precipitation

Lastly, we investigate if curtains are drifting or locally precipitating. Figure 6a shows a map of the northern BLC region in the North Atlantic. The solid blue line is the northern boundary where an electron that mirrors locally at 700 km has a conjugate mirror point at 100 km in the SAA. Immediately south of the solid blue line, the conjugate mirror altitude rapidly decreases towards, and below, sea level. The dashed blue line is the boundary where the conjugate mirror point altitude is at sea level. South of this line the

[c1] ~~($L \approx 5 - 8$)~~
[c2] *Text added.*
[c3] *Text added.*
[c4] *Text added.*
[c5] *Text added.*
[c6] *Text added.*
[c7] *Text added.*
[c8] *Text added.*
[c9] *Text added.*
[c10] *Text added.*
[c11] *Text added.*

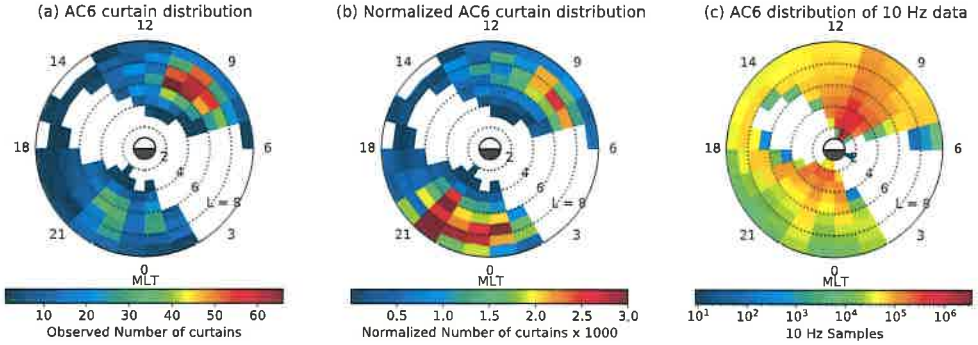

Figure 3. The distribution of observed curtains by L shell and MLT. Panel a shows the locations of all observed curtains used in this study. Panel b shows the curtain distribution normalized by the number of quality 10 Hz samples taken in each bin, shown in panel c. The white bins in panels a and b show where no curtains were observed, while in panel c the white bins show where AC6 did not take any 10 Hz data at the same location.

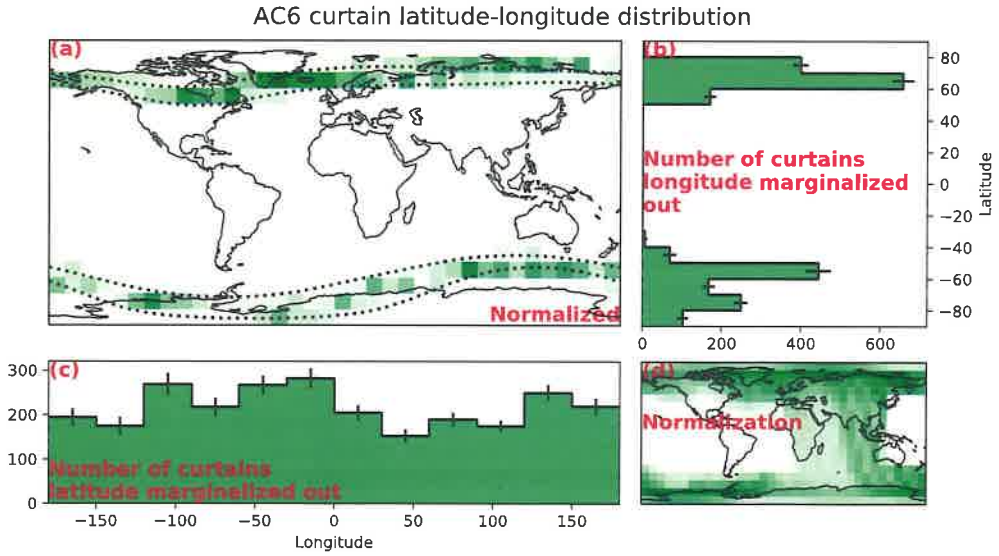

Figure 4. The geographic distribution of curtains. Panel a shows a map of the normalized number of curtains, normalized by the number of 10 Hz samples that AC6 took a the same location, shown in panel d. The dotted black lines in panel a shows the L=4 and L=10 contours. Panels b and c show the marginalized and normalized distribution of curtains in latitude and longitude, respectively. The error bars in panels b and c are the standard errors derived assuming Poisson statistics.

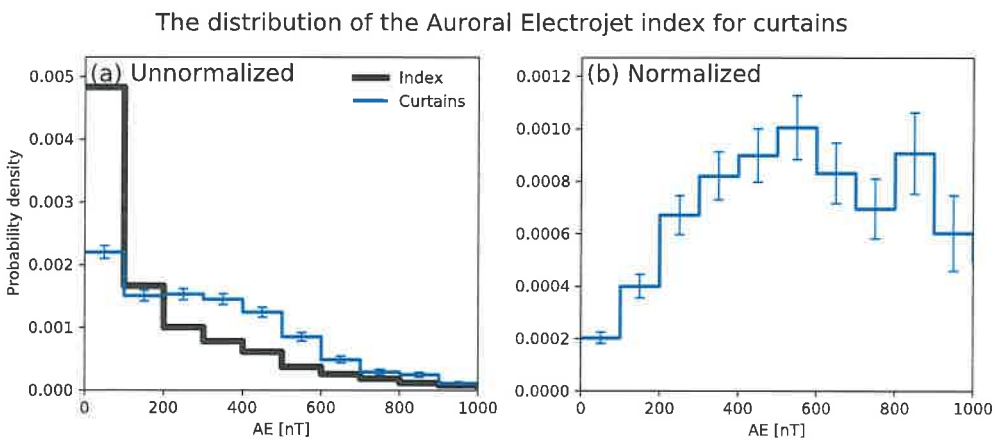

Figure 5. The distribution of the Auroral Electrojet (AE) index when curtains were observed. The blue line in panel a shows the distribution of AE when curtains where observed, and for reference the black line is shows the distribution of the AE index between 2014 and 2017 when quality 10 Hz data is available from both AC6 spacecraft. Panel b shows the curtain distribution normalized by the AE index distribution, and it represents the distribution assuming that any AE index is equally probable. The error bars are derived assuming the Poisson standard error.

conjugate mirror point is inside the Earth. For reference, AC6 takes about 30 seconds to move between the solid and dashed blue curves. The two dotted black curves in Fig. 6a are roughly the boundary of the outer radiation belt, defined as L = 4 – 8.

Of the 1,634 curtains, we found 36 curtains that were observed inside the BLC region. Figure 6b-e shows 4 curtain examples (AC6-B time shifted by the in-track lag), along with the AC6 in-track lag, L and MLT during the observations annotated. The AC6 locations where these curtains were observed are shown in Fig. 6a with the red stars and the corresponding panel labels. [c1] Recall from section 3.2 [c2] that in this region, all particles that can access AC6, regardless of their pitch angle, were in the bounce loss cone. ~~They were not drifting.~~

I and would be lost within 1/2 bounce period.

5 Discussion

5.1 Curtain Width

Curtains are narrow in latitude. Figure 2 shows that the width of most curtains is on the order of 1 – 3 seconds in time as observed by AC6, corresponding to a 8 – 20 kilometer spatial width along the AC6 orbit track. The reduced sensitivity of the detection algorithm, as described in Section 3.1, is unlikely to significantly underestimate the curtain width distribution because most curtains had a width less than half of the 10-second baseline's width. Scaled to the magnetic equator, the curtain widths correspond to a source with a radial scale size of a few hundred kilometers. The curtains with a < 1 second duration suggest that past microburst observations could have been mistaken for curtains, so the microburst impact on the atmosphere and the radiation belt is overestimated.

[c1] *Text added.*
[c2] *Text added.*

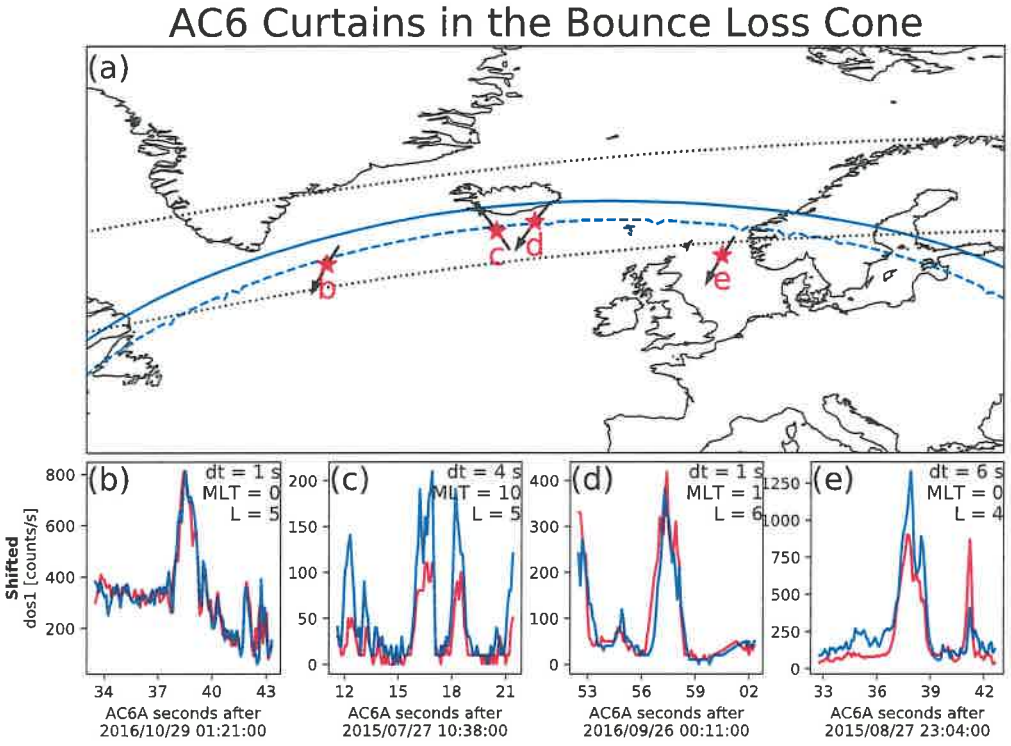

Figure 6. Curtains observed in the bounce loss cone region. Panel a shows a map of the North Atlantic region with the outer radiation belt, defined by $L = 4 - 8$, shown with the dotted black curves. The solid blue curve shows the northern boundary of the bounce loss cone region. Along this curve, electrons locally mirroring at 700 kilometers altitude have a conjugate mirror point at 100 kilometers altitude in the SAA. A more strict bounce loss cone criterion is the dashed blue curve that represents a conjugate mirror point altitude at sea level in the SAA. The 4 red stars with labels show the locations of the curtain examples shown in the corresponding panels b-e. In panel a, the black curves with arrows that pass through the red stars show one minute of AC6's orbit path and direction. The panels b-e show the 4 example curtains with the AC6-A data shown by the red line and the time-shifted AC6-B data with the blue line. The annotations in each example show the AC6 in-track lag (dt), L, and MLT rounded to the nearest integer. AC6-A was leading in all examples except in panel d.

↳ shouldn't dt be -1 s then?
Is it coincidence that all are integer time shifts?

As shown in Fig. 1, it is remarkable that some curtains maintain a fine structure after multiple seconds with little observable difference. However, sometimes curtains appear to be slightly and systematically shifted in latitude, while maintaining their fine structure (not shown).

5.2 When and Where Are Curtains Observed

Figure 3b shows that curtains likely originate in the outer radiation belt [c1]or the plasma sheet and are observed relatively more in the pre-midnight than late-morning MLT regions. [c2]The MLT distribution is biased by AC6's orbit and curtains are very likely to exist inside the sizable sampling gaps in Fig. 3c. Furthermore, curtains are more often observed at higher L shells near midnight MLT, however the sampling statistics at high L are limited because AC6 rapidly crosses high L shells. [c3]

[c4]The curtain distribution in longitude, shown in Fig. 4c, [c5]does not show a clear trend in longitude. If curtains were drifting, the number of curtains will increase to the East of the SAA to a maximum at the Western edge of the SAA. Thus, it is unlikely that curtains are drifting.

Lastly, Figure 5b shows that curtains are associated with an enhanced AE up to around 600 nT. While it is not a direct comparison (due to the electron energy channels and the binning scheme), Douma et al. (2019) showed that the number of microburst observed by SAMPEX increases with increasing AE, up to about AE = 300 nT.

5.3 Curtains Observed in The Bounce Loss Cone

The handful of curtains observed in the bounce loss cone, and shown in Fig. 6, put the Blake and O'Brien (2016) curtain drift hypothesis into question. These curtains were observed near the sea level mirror altitude curve. One possible explanation is that the drifting curtain electrons were observed at the end of their drift orbit, however because these examples were seen far from the western edge of the BLC, any drifting electrons would have been lost before AC6 observed them. Thus, they were not drifting and were precipitating for as long as 6 seconds, as shown in Fig. 6e. The curtain precipitation persisted for multiple bounce periods ($\approx$ 1.5 seconds for 35 keV electrons in this region), suggesting that the curtain generation mechanism must be capable of persistently scattering electrons. [c6]This rules out chorus waves as the source of these curtains, and we will now consider the second hypothesized mechanism introduced in section 1.

5.4 An Alternative Curtain Generation Mechanism

DC or quasi DC or static or quasi static

[c7] One candidate mechanism, [c8]that can generate curtains, is a direct current electric field that is parallel to the background magnetic field, that lowers the electron mirror point to AC6 altitudes. To find the minimum potential we assume the electron is barely trapped and has a 100-kilometer conjugate mirror point altitude in the SAA, so initially the electron will mirror above AC6 in the bounce loss cone region.

[c1] *Text added.*
[c2] *Text added.*
[c3] ~~Nevertheless, Fig. 3b hints that curtains near midnight MLT were observed at L shells possibly outside the outer radiation belt.~~
[c4] *Text added.*
[c5] *Text added.*
[c6] *Text added.*
[c7] ~~The scattering mechanism must be radially localized; if we assume the mechanism is at the magnetic equator, it must be on a scale of a few hundred kilometers.~~
[c8] *Text added.*

To find the parallel potential, $q\Phi$, we use the kinetic energy, W, of a 35 keV electron at its initial mirror point with a magnetic field strength of B_i. The kinetic energy at the initial mirror point can be written as $W_i = \mu B_i$ where μ is the first adiabatic invariant that is conserved during this acceleration. When a parallel potential accelerates the electron of charge q and does $q\Phi$ amount of work, the electron will mirror closer to Earth's surface and mirror at a field strength B_f where its final energy is $W_f = \mu B_f$. Now we relate the initial and final kinetic energy of the electron,

$$\mu B_f = \mu B_i + q\Phi. \tag{1}$$

Then we solve for $q\Phi$ and substitute μ to express the above equation as a function of the initial kinetic energy

$$q\Phi = W_i \frac{(B_f - B_i)}{B_i}. \tag{2}$$

The parallel potential is proportional to W_i so a larger potential is necessary to accelerate higher energy electrons. AC6 dos1 electron energy response increases rapidly from 30 keV to a peak at 100 keV (Figure 2 in O'Brien et al., 2019), therefore our assumption that $W_i = 35$ keV can underestimate the parallel potential. Nevertheless, the counts observed by AC6 are a convolution of, among other things, the AC6 dos1 electron energy response and the falling electron energy spectrum. Thus, the majority of electrons that AC6 observed have energies close to 35 keV and the $W_i = 35$ keV is an appropriate approximation.

We again used [c1]the Olson-Pfitzer magnetic field model to estimate $q\Phi$. For each example curtain in Fig. 6, we first estimated the local magnetic field, B_f, that the electron descended to after the acceleration. Then we traced the local field line into the SAA. We estimated B_i at 100 kilometers altitude in the SAA for barely trapped electrons. With the initial and final B, along with $W = 35$ keV, the minimum potential was between $q\Phi = 1 - 4$ kV for the examples shown in Fig. 6.

The range of estimated potentials is typical for the inverted-V discrete aurora. Partamies et al. (2008), using observations made by the Fast Auroral SnapshoT (FAST) mission, reported that auroral inverted-V electron precipitation structures, with electron energies up to a few tens of keV, were accelerated by 2-4 kV parallel potentials. The inverted-V structure and curtains share several similarities including: latitudinal width, high occurrence rate in the midnight MLT region, and the maximum inverted-V energy extends into tens of keV (e.g. Marklund et al., 2011; Thieman & Hoffman, 1985). AC6's dos1, with its 35 keV electron threshold, may by observing the highest energy tip of the inverted-V aurora. A possible connection between the inverted-V structures is intriguing, but by itself AC6 cannot easily test this hypothesis. To investigate further, a follow-on study could look at ground-based auroral imager data and look for meso-scale auroral arcs when AC6 observed curtains overhead.

Regardless of the source of the curtain precipitation, the impact of curtains on the atmosphere needs to be quantified. Even if the curtains observed in the BLC are the exception and other curtains are drifting, the drifting curtains will still precipitate within one drift period. Precipitating electrons produce odd reactive nitrogen (NO_X) molecules that are currently underestimated by atmospheric models such as the widely-used Whole Atmosphere Community Climate Model (WACCM) (e.g. Randall et al., 2015). Curtain precipitation could explain the lack of atmospheric NO_X. An AC6-like mission with pitch angle and energy resolution will be necessary to quantify the curtain impact on the atmosphere.

[c1] ~~IRBEM-Lib~~

6 Conclusions

The 1,634 curtains examined here allowed us to make the following inferences:

1. Curtains are narrow—90% are less than 20 kilometers wide in the latitudinal direction.
2. [c1] Considering AC6's sampling bias to the pre-midnight and pre-noon MLT regions, curtains were relatively more often observed in the pre-midnight MLT region than the pre-noon MLT region [c2]
3. [c3] Curtains occur relatively more frequently during active geomagnetic periods.
4. Some curtains continuously precipitate into the atmosphere for multiple seconds, [c4] limited by AC6's short in-track lag.

pre-midnight seems overly broad here since peak normalized bin is actually IN a low measurement hour.

at least

As shown in Fig. 1, curtain precipitation is narrow with a fine structure that persists for multiple seconds: for at least 26 seconds as shown in Fig. 1d. Either the scattering mechanism that continuously generates curtains is physically static for multiple seconds, or the curtain electron drift is often undisturbed.

Evidence for,

The curtain-microburst relationship hypothesized in Blake and O'Brien (2016) is not clear. Curtains observed in the bounce loss cone cast doubt on the curtain-microburst hypothesis. Some curtains continuously precipitate for at least a few seconds, and can be a significant source of energetic electron precipitation into the atmosphere. Lastly, we found that the continuous scattering of curtain electrons can be explained by a parallel direct current electric field, possibly relating curtains to the aurora.

Appendix A Distribution of Colocated 10 Hz Data

Figure A1 shows the distribution of colocated AC6 10 Hz data as a function of in-track lag. This distribution is heavily dominated by small in-track lags and 72% of the colocated 10 Hz data was taken when AC6 was separated in-track by less than 10 seconds, corresponding to 75 km in-track separation. Therefore, most of the curtains studied here were observed for small in-track lags, which limits our ability to explore the extent of the curtain duration.

Appendix B Estimating Curtain Widths

The curtain width in the dos1 time series is defined here as the width at half of the curtain's topographic prominence. Topographic prominence for a peak in a time series is the height of a peak relative to the maximum of the two minima on either side of the peak. The minima on either side of the peak are searched for between the peak and the nearest higher peak on that side. Figure B1 shows 5 examples of curtains observed by AC6-A in red (for clarity the AC6-B data is not shown), and the curtain width is shown by the horizontal black line.

Acknowledgments

This work was made possible with the help from the many engineers and scientists at The Aerospace Corporation who designed, built, and operated AC6. M. Shumko was supported by NASA Headquarters under the NASA Earth and Space Science Fellowship Pro-

[c1] *Text added.*

[c2] ~~Curtains are observed predominately in the pre-midnight MLT region, and during active geomagnetic periods.~~

[c3] *Text added.*

[c4] *Text added.*

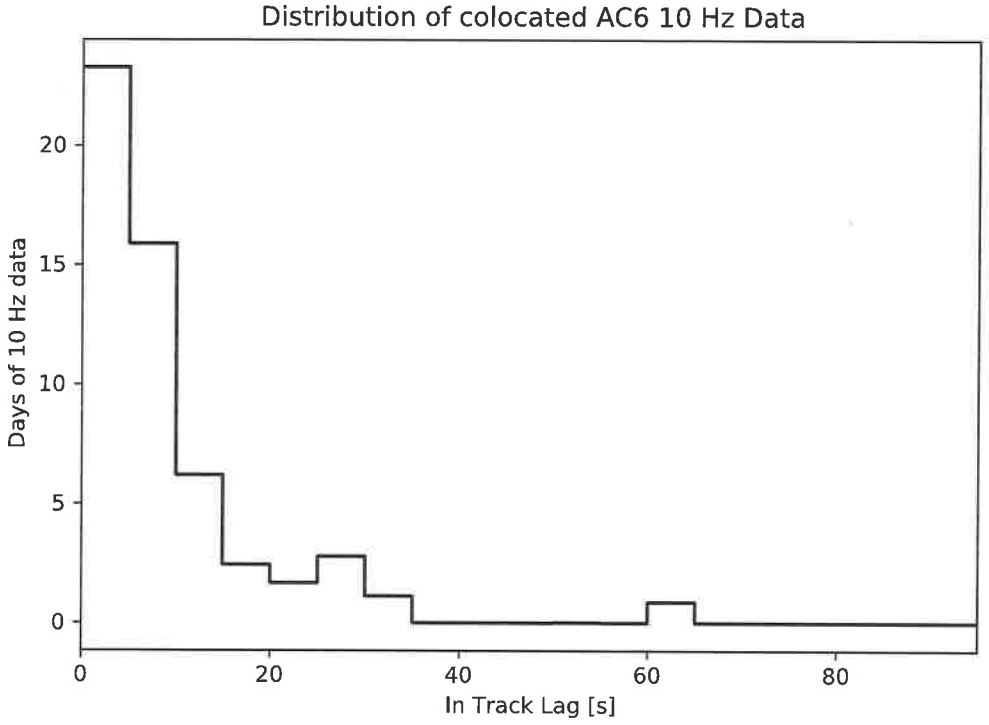

Figure A1. The distribution of colocated 10 Hz data as a function of in-track lag. Bins are 5 seconds wide.

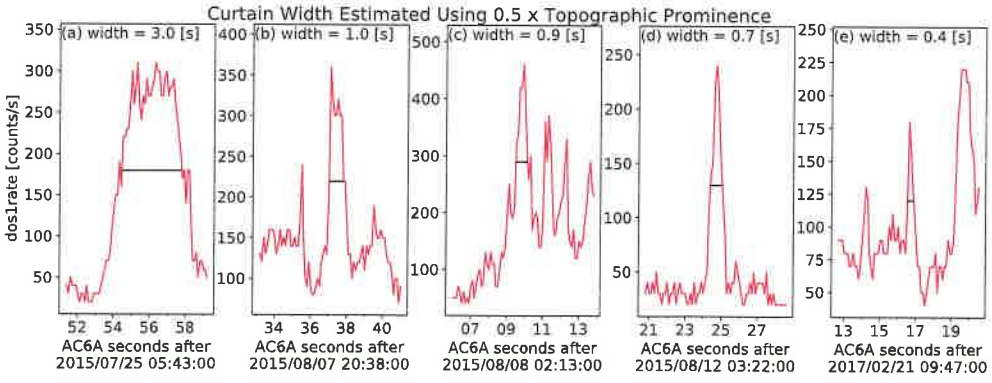

Figure B1. Five examples of curtains observed by AC6A shown with the red curves and the curtain widths are shown with the horizontal black lines and annotated. The height of the horizontal black lines are at half of the curtain's topographic prominence.

gram - Grant 80NSSC18K1204 and NASA Postdoctoral Program at the NASA's Goddard Space Flight Center, administered by Universities Space Research Association under contract with NASA. D.L. Turner is thankful for funding from a NASA grant (prime award number: 80NSSC19K0280). The work at The Aerospace Corporation was supported in part by RBSP-ECT funding provided by JHU/APL contract 967399 under NASA's Prime contract NAS501072. The AC6 data and documentation is available at http://rbspgway.jhuapl.edu/ac6 and the IRBEM-Lib version used for this analysis can be downloaded from https://sourceforge.net/p/irbem/code/616/tree/. [c1]The 1-minute cadence provisional AE index data was downloaded from http://wdc.kugi.kyoto-u.ac.jp/aeasy/

References

Anderson, B., Shekhar, S., Millan, R., Crew, A., Spence, H., Klumpar, D., ... Turner, D. (2017). Spatial scale and duration of one microburst region on 13 August 2015. *Journal of Geophysical Research: Space Physics*.

Anderson, K. A., & Milton, D. W. (1964). Balloon observations of X rays in the auroral zone: 3. High time resolution studies. *Journal of Geophysical Research*, *69*(21), 4457–4479. Retrieved from `http://dx.doi.org/10.1029/JZ069i021p04457` doi: 10.1029/JZ069i021p04457

Blake, J. B., Looper, M. D., Baker, D. N., Nakamura, R., Klecker, B., & Hovestadt, D. (1996). New high temporal and spatial resolution measurements by sampex of the precipitation of relativistic electrons. *Advances in Space Research*, *18*(8), 171 - 186. Retrieved from `http://www.sciencedirect.com/science/article/pii/0273117795009698` doi: http://dx.doi.org/10.1016/0273-1177(95)00969-8

Blake, J. B., & O'Brien, T. P. (2016). Observations of small-scale latitudinal structure in energetic electron precipitation. *Journal of Geophysical Research: Space Physics*, *121*(4), 3031–3035. Retrieved from `http://dx.doi.org/10.1002/2015JA021815` (2015JA021815) doi: 10.1002/2015JA021815

Blum, L., Li, X., & Denton, M. (2015). Rapid MeV electron precipitation as observed by SAMPEX/HILT during high-speed stream-driven storms. *Journal of Geophysical Research: Space Physics*, *120*(5), 3783–3794. Retrieved from `http://dx.doi.org/10.1002/2014JA020633` (2014JA020633) doi: 10.1002/2014JA020633

Blum, L., Schiller, Q., Li, X., Millan, R., Halford, A., & Woodger, L. (2013). New conjunctive cubesat and balloon measurements to quantify rapid energetic electron precipitation. *Geophysical research letters*, *40*(22), 5833–5837.

Boscher, D., Bourdarie, S., O'Brien, P., Guild, T., & Shumko, M. (2012). *Irbem-lib library*.

Breneman, A., Crew, A., Sample, J., Klumpar, D., Johnson, A., Agapitov, O., ... others (2017). Observations directly linking relativistic electron microbursts to whistler mode chorus: Van allen probes and FIREBIRD II. *Geophysical Research Letters*.

Brown, J., & Stone, E. (1972). High-energy electron spikes at high latitudes. *Journal of Geophysical Research*, *77*(19), 3384–3396.

Brown, R., Barcus, J., & Parsons, N. (1965, 6). Balloon observations of auroral zone x rays in conjugate regions. 2. microbursts and pulsations. *Journal of Geophysical Research (U.S.)*, *70*. doi: 10.1029/JZ070i011p02599

Comess, M., Smith, D., Selesnick, R., Millan, R., & Sample, J. (2013). Duskside relativistic electron precipitation as measured by sampex: A statistical survey. *Journal of Geophysical Research: Space Physics*, *118*(8), 5050-5058. Retrieved from `https://agupubs.onlinelibrary.wiley.com/doi/abs/`

[c1] *Text added.*

10.1002/jgra.50481 doi: 10.1002/jgra.50481

Crew, A. B., Spence, H. E., Blake, J. B., Klumpar, D. M., Larsen, B. A., O'Brien, T. P., ... Widholm, M. (2016). First multipoint in situ observations of electron microbursts: Initial results from the NSF FIREBIRD II mission. *Journal of Geophysical Research: Space Physics*, *121*(6), 5272–5283. Retrieved from http://dx.doi.org/10.1002/2016JA022485 (2016JA022485) doi: 10.1002/2016JA022485

Dietrich, S., Rodger, C. J., Clilverd, M. A., Bortnik, J., & Raita, T. (2010). Relativistic microburst storm characteristics: Combined satellite and ground-based observations. *Journal of Geophysical Research: Space Physics*, *115*(A12).

Douma, E., Rodger, C., Blum, L., O'Brien, T., Clilverd, M., & Blake, J. (2019). Characteristics of relativistic microburst intensity from sampex observations. *Journal of Geophysical Research: Space Physics*.

Douma, E., Rodger, C. J., Blum, L. W., & Clilverd, M. A. (2017). Occurrence characteristics of relativistic electron microbursts from SAMPEX observations. *Journal of Geophysical Research: Space Physics*, *122*(8), 8096–8107. Retrieved from http://dx.doi.org/10.1002/2017JA024067 (2017JA024067) doi: 10.1002/2017JA024067

Greeley, A., Kanekal, S., Baker, D., Klecker, B., & Schiller, Q. (2019). Quantifying the contribution of microbursts to global electron loss in the radiation belts. *Journal of Geophysical Research: Space Physics*.

Hoffman, R. A., & Evans, D. S. (1968). Field-aligned electron bursts at high latitudes observed by ogo 4. *Journal of Geophysical Research*, *73*(19), 6201–6214.

Imhof, W., Voss, H., Mobilia, J., Datlowe, D., & Gaines, E. (1991). The precipitation of relativistic electrons near the trapping boundary. *Journal of Geophysical Research: Space Physics*, *96*(A4), 5619–5629.

Johnson, A., Shumko, M., Griffith, B., Klumpar, D., Sample, J., Springer, L., ... others (2020). The FIREBIRD-II CubeSat mission: Focused investigations of relativistic electron burst intensity, range, and dynamics. *Review of Scientific Instruments*, *91*(3), 034503.

Lehtinen, N. G., Inan, U. S., & Bell, T. F. (2000). Trapped energetic electron curtains produced by thunderstorm driven relativistic runaway electrons. *Geophysical research letters*, *27*(8), 1095–1098.

Lorentzen, K. R., Blake, J. B., Inan, U. S., & Bortnik, J. (2001). Observations of relativistic electron microbursts in association with VLF chorus. *Journal of Geophysical Research: Space Physics*, *106*(A4), 6017–6027. Retrieved from http://dx.doi.org/10.1029/2000JA003018 doi: 10.1029/2000JA003018

Lorentzen, K. R., Looper, M. D., & Blake, J. B. (2001). Relativistic electron microbursts during the GEM storms. *Geophysical Research Letters*, *28*(13), 2573–2576. Retrieved from http://dx.doi.org/10.1029/2001GL012926 doi: 10.1029/2001GL012926

Marklund, G. T., Sadeghi, S., Cumnock, J. A., Karlsson, T., Lindqvist, P.-A., Nilsson, H., ... others (2011). Evolution in space and time of the quasi-static acceleration potential of inverted-v aurora and its interaction with alfvénic boundary processes. *Journal of Geophysical Research: Space Physics*, *116*(A1).

Meredith, N. P., Horne, R. B., Shen, X.-C., Li, W., & Bortnik, J. (2020). Global model of whistler mode chorus in the near-equatorial region ($|\lambda_m| < 18°$). *Geophysical Research Letters*, *47*(11), e2020GL087311.

Millan, R., & Thorne, R. (2007). Review of radiation belt relativistic electron losses. *Journal of Atmospheric and Solar-Terrestrial Physics*, *69*(3), 362 - 377. Retrieved from //www.sciencedirect.com/science/article/pii/S1364682606002768 doi: http://dx.doi.org/10.1016/j.jastp.2006.06.019

O'Brien, T. P., Blake, J. B., & W., G. J. (2016, May). *AeroCube-6 dosimeter data README* (Tech. Rep. No. TOR-2016-01155). The Aerospace Corporation.

O'Brien, T. P., Looper, M. D., & Blake, J. B. (2019, July). *AeroCube-6 dosimeter equivalent energy thresholds and flux conversion factors* (Tech. Rep. No. TOR-2017-02598). The Aerospace Corporation.

O'Brien, T. P., Lorentzen, K. R., Mann, I. R., Meredith, N. P., Blake, J. B., Fennell, J. F., ... Anderson, R. R. (2003). Energization of relativistic electrons in the presence of ULF power and MeV microbursts: Evidence for dual ULF and VLF acceleration. *Journal of Geophysical Research: Space Physics*, *108*(A8). Retrieved from http://dx.doi.org/10.1029/2002JA009784 doi: 10.1029/2002JA009784

Olson, W. P., & Pfitzer, K. A. (1982). A dynamic model of the magnetospheric magnetic and electric fields for july 29, 1977. *Journal of Geophysical Research: Space Physics*, *87*(A8), 5943–5948. Retrieved from http://dx.doi.org/10.1029/JA087iA08p05943 doi: 10.1029/JA087iA08p05943

Parks, G. K. (1967). Spatial characteristics of auroral-zone X-ray microbursts. *Journal of Geophysical Research*, *72*(1), 215–226.

Partamies, N., Donovan, E., & Knudsen, D. (2008). Statistical study of inverted-v structures in fast data. In *Annales geophysicae* (Vol. 26, pp. 1439–1449).

Randall, C. E., Harvey, V. L., Holt, L. A., Marsh, D. R., Kinnison, D., Funke, B., & Bernath, P. F. (2015). Simulation of energetic particle precipitation effects during the 2003–2004 arctic winter. *Journal of Geophysical Research: Space Physics*, *120*(6), 5035–5048.

Selesnick, R. S., Blake, J. B., & Mewaldt, R. A. (2003). Atmospheric losses of radiation belt electrons. *Journal of Geophysical Research: Space Physics*, *108*(A12). Retrieved from http://dx.doi.org/10.1029/2003JA010160 (1468) doi: 10.1029/2003JA010160

Seppälä, A., Douma, E., Rodger, C., Verronen, P., Clilverd, M. A., & Bortnik, J. (2018). Relativistic electron microburst events: Modeling the atmospheric impact. *Geophysical Research Letters*, *45*(2), 1141–1147.

Shumko, M., Johnson, A., Sample, J., Griffith, B. A., Turner, D. L., O'Brien, T. P., ... Claudepierre, S. G. (2020). Electron microburst size distribution derived with AeroCube-6. *Journal of Geophysical Research: Space Physics*, e2019JA027651.

Thieman. J. R., & Hoffman, R. A. (1985). Determination of inverted-v stability from dynamics explorer satellite data. *Journal of Geophysical Research: Space Physics*, *90*(A4), 3511–3516.

Thorne, R. M., O'Brien, T. P., Shprits, Y. Y., Summers, D., & Horne, R. B. (2005). Timescale for MeV electron microburst loss during geomagnetic storms. *Journal of Geophysical Research: Space Physics*, *110*(A9). Retrieved from http://dx.doi.org/10.1029/2004JA010882 (A09202) doi: 10.1029/2004JA010882

Tsyganenko, N. (1989). A solution of the chapman-ferraro problem for an ellipsoidal magnetopause. *Planetary and Space Science*, *37*(9), 1037 - 1046. Retrieved from http://www.sciencedirect.com/science/article/pii/0032063389900767 doi: http://dx.doi.org/10.1016/0032-0633(89)90076-7